

Supplementary Information to “Spontaneous synchronization driven by energy transport in interconnected networks”

Vincenzo Nicosia,^{1,*} Per Sebastian Skardal,^{2,*} Vito Latora,¹ and Alex Arenas²

¹*School of Mathematical Sciences, Queen Mary University of London*

²*Department d'Enginyeria Informàtica i Matemàtiques, Universitat Rovira i Virgili*

Understanding dynamical processes on networks is an important area of research in complex systems, with far reaching implications and applications in many real-world cases. However, the research to date has mainly focused on single dynamical processes occurring on isolated networks, and very little is known about the more interesting and realistic case of different kinds of intertwined dynamical processes taking place on interconnected networks. An example of the non-trivial combination of two types of dynamics can be found in the human brain, where cerebral circulation delivers the nutrients and oxygenated blood needed for the activity of the different brain areas, and in turn the activity of a region can induce changes in the distribution of blood flow. Here, we introduce and study a model of intertwined dynamics on interconnected networks, inspired by the human brain, which consists of bidirectionally coupled synchronization and energy transport processes. Remarkably, the proposed model allows the emergence of spontaneous switch-like synchronization transitions driven by the energy transport dynamics, which qualitatively mirror the transitions observed in human brain dynamics between resting-state and cognitive activity. We provide a steady-state analytical explanation for the observed behavior and furthermore show that the switch-like transition is robust over a wide range of model parameters and network topologies. We suggest that the complexity inherent in other interconnected dynamical processes might be responsible for various other emergent behaviors observed in natural systems.

I. INTRODUCTION

A large variety of natural and man-made systems, from societies to the human brain, consist of many elementary dynamical units coupled through a complex network of interactions [1, 2], which often give rise to the spontaneous emergence of collective behaviors [3]. In the last two decades, network science has extensively shown that the structure of the network is often responsible for the dynamics and stability of such emerging behaviors [4–8]. However, dynamical processes in nature do not evolve in absolute isolation, and real-world systems are usually characterized by several intertwined and co-evolving dynamics, happening at different levels and developing over different temporal scales. A wonderful example of this kind of multi-level complexity is the human brain, whose activity is the combination of several dynamics, including blood flow, oxygen exchange, chemical and electrical interactions among neurons, and remote synchronization of distant regions [9–11]. In this case, the behavior of the system is clearly determined by the co-evolution of various dynamical processes which take place on different networks and are interconnected by relationships of different nature. However, apart from a few recent studies [12, 13], to date the topic of intertwined dynamical processes on interconnected networks remains largely unexplored, mainly due to the intrinsic complexity of dealing with different dynamical processes coupled through distinct types of interactions.

In this Article we propose a mathematical formula-

tion of the problem based on a multiplex networks approach [14, 15] in which the interactions among nodes are grouped in different categories and are modeled as the distinct layers of the network. We focus our attention on the case of two intertwined processes, namely energy transport and synchronization dynamics, which mimic the interplay between neural activity and blood and oxygen abundance in brain regions. We show that the coupling of the two processes gives rise to a novel mechanism of spontaneous switch-like synchronization controlled by the transport of energy. The behavior found in the model is surprisingly similar to the transitions observed in human brain function between resting-states and cognitive activities [10], as well as to other spontaneous transition phenomena observed in other biological systems [16–19].

II. MODEL DESCRIPTION

A. Multiplex structure

The evolution of inter-dependent dynamics characterized by different interconnection patterns can be naturally described with multiplex networks. This framework was initially developed in social network analysis [20, 21] and has been recently extended to the modeling of multi-level complex systems of different kinds [22–25]. In general, a multiplex network consists of a set of N nodes and L layers, in which links in different layers typically represent different kinds of interactions between the nodes. Each node exists in all the layers, but in general each single layer has a distinct topology, so that the local connectivity of each node differs across layers. In this paper we consider a multiplex consisting of two layers: a

*These authors contributed equally to this work

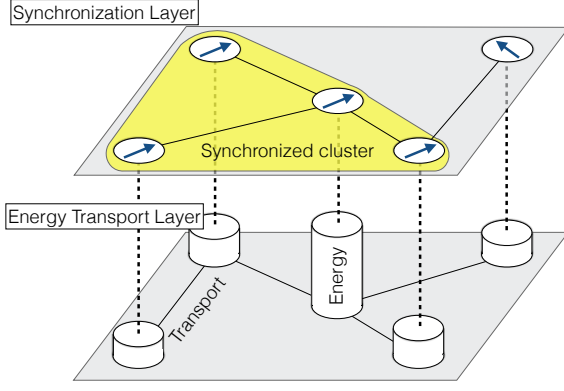


FIG. 1: **Interdependent dynamics on multiplex networks.** Illustration of a multiplex with two layers accounting, respectively, for the synchronization of coupled Kuramoto oscillators and for the transport of random walkers (energy packets). Note that there is a one-to-one correspondence between the nodes in each layer, while each layer has different connectivity properties, so that a node i has degree q_i at the first layer and k_i at the second. The state of a node i at a given time t is characterized by the phase $\theta_i(t)$ of the oscillator at the synchronization layer and by the probability p_i^t of finding a walker at node i on the transport network. The two processes, transport and synchronization, are coupled in such a way that the synchronization dynamics at a node depends on its availability of energy (namely the oscillator frequency of a node in the synchronization layer is proportional to the available energy in the transport layer) and, at the same time, the motion of energy in the transport layer is biased according to the degree of the node in the synchronization network.

synchronization layer and an *energy transport* layer. The adjacency matrices encoding the synchronization and energy transport layers, which we assume for simplicity are undirected and unweighted, are denoted $A = \{a_{ij}\}$ and $E = \{e_{ij}\}$, respectively. Additionally, we denote the degree of node i in the synchronization and energy transport layers $k_i = \sum_{j=1}^N a_{ij}$ and $q_i = \sum_{j=1}^N e_{ij}$, respectively.

In Fig. 1 we illustrate the structure of the multiplex with the synchronization layer (top) and the energy transport layer (bottom), where we wanted to stress the fact that, despite each node is present in both layers, the network topology in each of two layers might in general be different. We will now describe in detail the dynamical processes occurring on both layers, and importantly, the bi-directional coupling between the two processes.

B. Energy transportation Layer

We model the transport of energy with a biased random walk process [26], in which a continuum of walkers, each interpreted as a “packet” of energy, moves throughout the network. Denoting the probability of finding a given random walker at node i (or equivalently, the fraction of all random walkers present at node i) at time t

by p_i^t , we consider the general random walk

$$p_j^{t+1} = \sum_{i=1}^N \pi_{ji} p_i^t, \quad (1)$$

where π_{ji} is the probability that a walker moves from node i to node j in a single time step. In this paper we consider the case where the random walk is biased on the degree k of the synchronization layer such that

$$\pi_{ji} = \frac{e_{ij} k_j^\alpha}{\sum_l e_{il} k_l^\alpha}. \quad (2)$$

Notice that a positive (negative) value of the bias parameter α will drive the walkers preferentially towards nodes with large (small) degree in the synchronization layer, while for $\alpha = 0$ we recover the classical unbiased random walk. The energy flow process is depicted in the bottom layer of Fig. 1, where the height of the white cylinder at each node is proportional to the number of energy packets available at that node. An important aspect of this model is that the movement of random walkers, and thus the occupation probability of energy packets at nodes, depends on the structure in both the energy transport and the synchronization layer.

C. Synchronization Layer

We model synchronization with an ensemble of N Kuramoto phase oscillators [6, 27]. Each node i is associated with a phase θ_i that evolves according to

$$\dot{\theta}_i = \omega_i + \lambda \sum_{j=1}^N a_{ij} \sin(\theta_j - \theta_i), \quad (3)$$

where ω_i is the natural frequency of oscillator i and λ is the coupling strength. Importantly, the dynamics of Eq. 3 is dependent on the dynamics in the energy transport layer through the natural frequencies. In particular, we assume that the natural frequency ω_i of oscillator i is proportional to the total energy (i.e., fraction of random walkers) present at node i in the energy transport layer. Without any loss of generality we set $\omega_i = N p_i$, so that the average natural frequency is equal to one. This choice is motivated by the fact that firing at a higher frequency usually requires a correspondingly higher amount of energy, in the form of oxygen and nutrients carried by blood [28].

To measure the degree of synchronization in the synchronization layer, we use the magnitude r of the complex Kuramoto order parameter, defined by

$$r e^{i\psi} = \frac{1}{N} \sum_{j=1}^N e^{i\theta_j}. \quad (4)$$

The order parameter in Eq. 4 thus represents the centroid of all the oscillators when placed appropriately on the

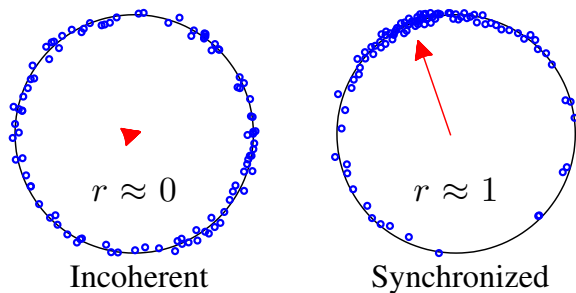


FIG. 2: **Synchronization order parameter.** Examples of incoherent (left) and synchronized (right) states of coupled oscillators. Oscillators are illustrated by small blue circles on the unit circle (with some randomly chosen offset for visualization), and each order parameter is illustrated by a large red vector arrow (see Eq. 4 for its definition). In the incoherent state oscillators are uniformly distributed about the circle, resulting in $r \approx 0$, while in the synchronized state the oscillators become entrained, resulting in $r \approx 1$.

complex unit circle. Consequently, $r \approx 0$ and $r \approx 1$ correspond, respectively, to incoherent and synchronized states.

The behavior of the order parameter for incoherent and synchronized states is depicted in Fig. 2. Oscillators are illustrated with small blue circles on the full unit circle (with some randomly chosen offset for visualization), while in each case the order parameter is illustrated with a large red vector arrow. The synchronization process is illustrated in Fig. 1 (top) where we represented oscillator phases with blue arrows and we highlight the synchronized cluster in yellow. We note that the frequency of each oscillator is proportional to the energy available (i.e., the height of the cylinder) at the corresponding node in the energy transport layer. The key element in our model is that each node of the system participates to both layers in such a way that synchronization and energy transport are naturally intertwined. Specifically, our choice of bidirectional coupling is inspired by studies that have confirmed the existence of relatively strong correlations between the electrical activity of a brain area and the hematic inflow in the same area, which is responsible for the transport of energy to the neurons in the form of oxygen molecules [29–31]. In our model the synchronization dynamics of a given node i depends on the availability of energy at i , and vice-versa the abundance of energy packets at node i depends on the participation in the synchronization layer.

III. RESULTS

A. Numerical simulations

We now show that the interplay of the two processes described above naturally produces a spontaneous switch-like synchronization transition controlled by the transport of energy on the bottom layer, even when the

topologies at the two layers are uncorrelated. Here we consider the simple case of a SF network in the synchronization layer and an ER random graph in the transport layer [32] with $N = 1000$ nodes each. The SF network is built using the configuration model [33] on a degree sequence drawn from a power-law distribution $P(k) \propto k^{-\gamma}$ with $\gamma = 2.8$ and enforced minimum degree $k_0 = 3$. For the ER network we used a link probability $p = 0.01$. The results are summarized in Fig. 3, for different values of the bias parameter α .

The main finding is the emergence of a spontaneous switch-like synchronization transition between incoherent and synchronized states. In Fig. 3 (a) we illustrate this phenomenon, plotting the steady-state order parameter r as a function of the coupling strength λ . In particular, we plot both the forward (fw, right-pointing red triangles) and backward (bw, left-pointing blue arrows) profiles, obtained by starting at $\lambda = 0$, slowly increasing its value until the system reached synchronization, and then slowly decreasing it again until zero. In particular, the profile is marked by first order phase transitions between two stable states (respectively, an incoherent and a synchronized state), and in the middle a bistable region/hysteresis loop (approximately $0.405 \lesssim \lambda \lesssim 0.457$). In the bistable region both the synchronized and the incoherent state are unstable, so that a large enough perturbation to the system and/or a temporary change in the value of λ yields a rapid transition to a different state. Consequently, in this regime the system effectively works like a switch.

To inspect the first-order transitions in more detail, we consider the long-time average effective frequency of each oscillator, defined as

$$\omega_i^{\text{eff}} = T^{-1} \int_{t_0}^{t_0+T} \dot{\theta}_i(t) dt, \quad (5)$$

for $T \gg 1$. In Fig. 3 (b), we report the average effective frequency of each oscillator as a function of λ as λ is increased. Note in particular the behavior immediately below and above the critical value $\lambda_c \simeq 0.457$. Below λ_c each oscillators' effective frequency is different, a mark of incoherent behavior. However, immediately above λ_c the majority of frequencies have collapsed onto the same value, $\omega_i^{\text{eff}} \simeq 1.0$, a mark of strongly synchronized behavior. In the inset we report the distribution of effective frequencies immediately below ($\lambda = 0.458$) and above ($\lambda = 0.456$) the critical value, noting that the former distribution is much wider than the latter one.

Finally, in Fig. 3 (c) we report the phase diagram of the system as a function of the bias parameter α and coupling strength λ . The steady-state degree of synchronization is indicated by color (incoherent and synchronized states correspond to blue and red, respectively), while the bistable region is indicated in white. It is interesting to notice that the bistable region is very robust and persists across a wide range of values of the bias parameter $0.6 < \alpha < 2.0$.

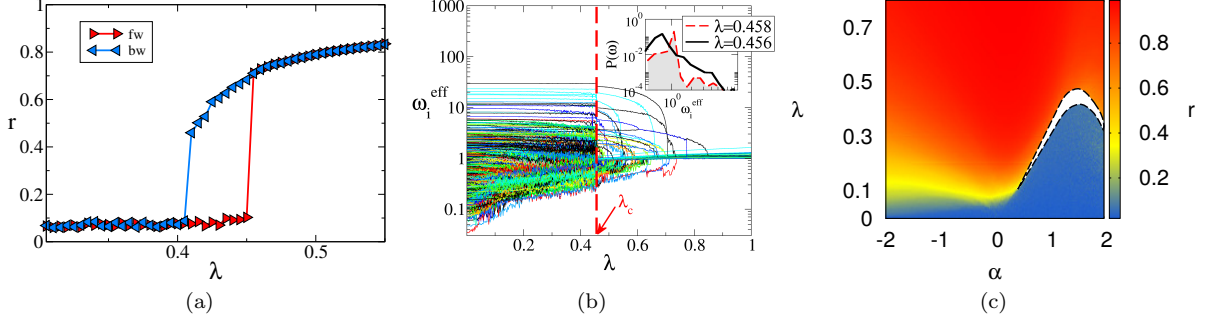


FIG. 3: **Intertwined dynamics foster spontaneous synchronization.** (a) Forward (red) and backward (blue) synchronization order parameter r as a function of the coupling strength λ for a multiplex system in which Kuramoto-like synchronization of oscillators on one layer is intertwined with energy transport modeled as an α -biased random walk ($\alpha = 1.4$) on the other layer. The transition to synchronization is abrupt and exhibits a hysteresis loop. (b) The spontaneous synchronization transition corresponds, at a microscopic level, to the sudden alignment of the effective frequencies ω_i^{eff} of an extensive fraction of the nodes, due to an infinitesimal increase of the coupling strength above the critical value $\lambda_c \simeq 0.457$, indicated by the dashed red line. The inset shows the distribution of ω_i^{eff} before (solid black line) and after the transition (dashed red line). (c) Phase diagram showing r as a function of α and λ . The white area bordered by dashed lines indicates the bistable region. Synchronization is explosive for $0.6 < \alpha < 2.0$. As α increases, the critical value of λ at which the system switches to the synchronized state increases up until $\alpha \simeq 1.5$, and then decreases again.

Spontaneous synchronization in the form of first-order explosive phase transitions has been found in a series of recent studies [34–36] where structural and dynamical correlations are artificially introduced in a single-layer network. Here, the appearance of an explosive synchronization transition is naturally due to the intertwined dynamics of energy transport and synchronization, and not to artificially imposed external constraints on the distribution of frequencies. Remarkably, we observe qualitatively similar behavior for several different combinations of network topologies in the synchronization and energy transport layers, in many cases resulting in robust parameter ranges that yield spontaneous switch-like synchronization transitions (see Appendix C for details).

B. Analytical results

Despite the intrinsic complexity of the system, the steady-state dynamics of the model can be well-described analytically, first by considering the random walker dynamics, then the synchronization dynamics. Given an initial distribution of random walkers \mathbf{p}^0 it can be shown that a unique stationary distribution $\mathbf{p}^* = \lim_{t \rightarrow \infty} \mathbf{p}^t$ exists provided that the network E is connected and has at least one odd cycle. In fact, given the biased movement rule in Eq. 2, the stationary distribution is given by [26]

$$p_i^* = \frac{k_i^\alpha \sum_{j=1}^N e_{ij} k_j^\alpha}{\sum_{l=1}^N k_l^\alpha \sum_{j=1}^N e_{lj} k_j^\alpha}, \quad (6)$$

a result we outline in Appendix A.

Given full information of both layers in the multiplex, one can directly compute the stationary distribution \mathbf{p}^*

from Eq. 6 or approximate it as follows. Assuming no structural correlations between the two layers the stationary probability at node i scales as a function of the local degrees in both layers, specifically, $p_i^* \propto k_i^\alpha q_i$. Moreover, if the transport layer is an ER graph, for which $q_i \approx \langle q \rangle = p(N-1)$, we obtain the even simpler approximation $p_i^* \propto k_i^\alpha$. This scaling is accurately reproduced by the simulations, as shown in Fig. 4 (a) for different values of α . It is also worth noticing that the value of the motion bias actually modifies the distribution of the natural frequencies of the oscillators. In the particular case of a SF synchronization layer with $P(k) \sim k^{-\gamma}$ we have that, on average, $P(\omega) \sim \omega^{-\gamma/\alpha}$, as shown in Fig. 4 (b).

The synchronization dynamics can also be described analytically using a self-consistency analysis. Given a set of frequencies defined by the random walker dynamics, $\omega_i = N p_i^*$, where p_i^* is given in Eq. 6, we construct the degree-frequency pair sequence $\{(k_i, \omega_i)\}_{i=1}^N$. Next, a lengthy heterogeneous mean-field analysis (presented in Appendix B) allows us to derive from Eq. 3, the self-consistency condition describing the approximate degree of synchronization r and the mean frequency of the synchronized cluster Ω :

$$r = \frac{\langle k \rangle^{-1}}{N} \sum_{|\omega_j - \Omega| \leq \lambda r k_j} k_j \sqrt{1 - \left(\frac{\omega_j - \Omega}{\lambda r k_j} \right)^2}, \quad (7)$$

$$\Omega = \frac{\sum_{|\omega_j - \Omega| \leq \lambda r k_j} \omega_j}{\sum_{|\omega_j - \Omega| \leq \lambda r k_j} 1}, \quad (8)$$

Equations (7) and (8) define r and Ω implicitly, however, can be solved using a simple iteration method. As shown in Fig. 4 (c), the expression of r given by Eq. 7 reproduces quite well the transition to synchronization.

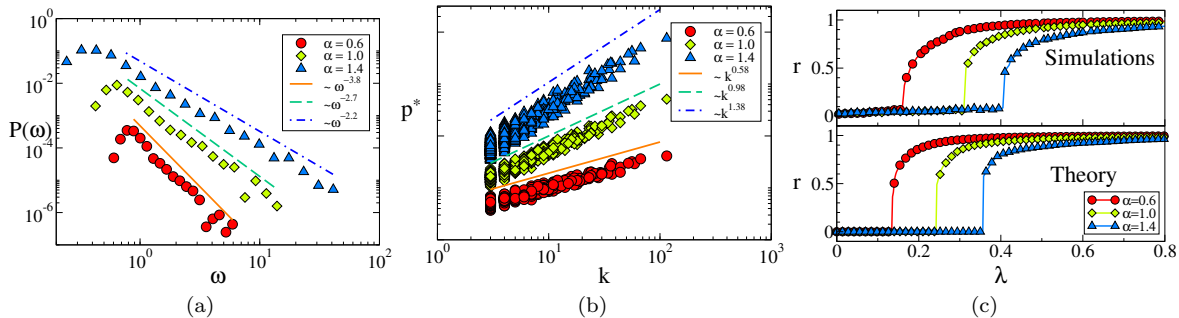


FIG. 4: **Agreement between theory and simulations.** (a) The value of the motion bias substantially affects the distribution of the oscillators' natural frequencies, so that smaller values of α correspond to more homogeneous distributions of ω_i , and vice-versa. In particular, when the transport layer is a random graph and the synchronization layer is a scale-free graph $P(k) \sim k^{-\gamma}$, we have $P(\omega) \sim k^{-\frac{\gamma}{\alpha}}$. (b) There is a clear correlation between the degree of a node on the synchronization layer and the natural frequency of the corresponding oscillator. In the simulations we observe $p_i^* \propto k_i^\alpha$, as expected. (c) The theory is also able to predict quite well the explosive transition to synchronization observed in the simulations. In particular, the value of r obtained by solving Eq. 7 for different values of λ (bottom panel) closely correspond to the backward synchronization diagrams of the simulated system (top panel). The plots in panel (a) and (b) were vertically displaced to enhance readability.

IV. DISCUSSION

Experimental studies have confirmed that the electrical activity registered in a brain area is very often correlated with the dynamics of hematic flow in the same region [29–31], and that in some cases the hematic inflow of a brain region can be indeed triggered by neuronal activity [37, 38]. However, mainstream research in neuroimaging has mostly focused so far on understanding each of these processes separately, by looking either at electroencephalographic/magnetoencephalographic signals (EEG/MEG) or at hematic signals (fMRI) [9]. Intriguingly, the spontaneous synchronization observed in our interconnected networks model closely mirrors that displayed by the human brain [10], which has the ability to very quickly switch between resting state activity, i.e., the background activity of a brain when no particular conscious task is performed, and complex intellectual and motor tasks [39].

Recent results based on different neuroimaging techniques seem to suggest that resting-state is not just the idle interval between two consecutive mental tasks, but is instead a particular configuration which is flexible enough to allow, upon the receipt of an appropriate exogenous stimulus, the quick and massive reconfiguration of brain activity needed for the performance of any particular task [10, 40–42]. This flexibility requires the availability of efficient switch-like mechanisms, as those exhibited by our model, in which either a slight perturbation of the rule governing energy distribution or a small increase in the strength of interaction among neurons, can easily induce a sudden, massive synchronization.

We find it quite remarkable that an efficient switch-like mechanism can naturally arise from the coupling of the two dynamics responsible for neural synchronization and energy transport, as shown by the model described in the paper. Indeed, each piece of the model is relatively simple, but the additional complexity introduced by the

intertwined dynamics results in an unexpected interesting behavior (i.e., spontaneous switch-like synchronization transitions) which is entirely driven by the energy transport process, and qualitatively mirrors similar transitions observed in the human brain. Despite this model of brain activity as the result of different interconnected and co-evolving dynamics exhibits some interesting properties, we believe that a more in-depth analysis of the relationship between hematic flow and neuronal activity is needed in order to provide a more in-depth understanding of brain functioning.

We would like to stress the fact that while human brain dynamics has been the main motivation of the present study, switch-like dynamics have been observed in many other biological processes also characterized by high levels of dynamical complexity [16–19]. We are convinced that the modeling approach proposed in this paper might help unravelling the complexity of these systems and could be useful to interpret their functioning as the result of a non-trivial combination of simpler underlying dynamical processes occurring on multilayer interdependent networks.

Acknowledgments

V.N. and V.L. acknowledge support from the EU-project LASAGNE (grant 318132), funded by the European Commission. P.S.S. and A.A. acknowledge support from the James S. McDonnell Foundation. A.A. acknowledges support by MINECO through Grant FIS2012-38266; f, the EU-project MULTIPLEX (grant 317532), the ICREA Academia program and the Generalitat de Catalunya 2009-SGR-838.

Appendix A: Derivation of the biased random walker stationary distribution

Here we follow Ref. [26] and derive the stationary distribution \mathbf{p}^* given by Eq. 6 for the biased random walker process described by Eqs. 1 and 2. The rule given by Eq. 2 is a specific case of the more generic rule:

$$\pi_{ji} = \frac{e_{ij} f_j}{c_i},$$

where f_j is an arbitrary function of the structural properties of node j (in our case taken to be $f_j = k_j^\alpha$), and $c_i = \sum_{j=1}^N e_{ij} f_j$. Next, we consider the probability of moving from node i to j in t time steps, denoted $P_{i \rightarrow j}(t)$, which is given by

$$P_{i \rightarrow j}(t) = \sum_{k_1, k_2, \dots, k_{t-1}} \pi_{jk_{t-1}} \times \dots \times \pi_{k_2 k_1} \times \dots \times \pi_{k_1 i}.$$

In particular, for undirected networks the ratio between the probabilities of traveling from node i to j and from node j to i in t time steps is

$$\frac{P_{i \rightarrow j}(t)}{P_{j \rightarrow i}(t)} = \frac{f_j c_j}{f_i c_i},$$

which, after rearranging and considering the stationary distribution \mathbf{p}^* , yields

$$f_i c_i p_i^* = f_j c_j p_j^*. \quad (\text{A1})$$

Finally, summing both sides of Eq. A1 over j and rearranging, we obtain

$$p_i^* = \frac{f_i c_i}{\sum_{j=1}^N f_j c_j}, \quad (\text{A2})$$

which is the more general expression for Eq. 6 given $f_i = k_i^\alpha$.

Appendix B: Derivation of the synchronization self-consistency condition

Here we derive from Eq. 3 the self consistency condition described by Eqs. 7 and 8 using a heterogeneous mean-field approach similar to that recently employed in Refs. [43, 44]. In the following analysis we assume a sufficiently large network and neglect any structural, e.g., degree-degree, correlations as well as any significant community structure. We will search for solutions consisting of a single synchronized cluster with $r > 0$ with constant angular velocity Ω . In many cases Ω can be reasonably approximated by the mean frequency $\Omega \approx \sum_i \omega_i / N$, however the following analysis results in an implicit expression for Ω that in principle needs to be solved self-consistently with r .

We begin by entering the rotating reference frame with (unspecified) angular velocity Ω by introducing the

change of variables $\phi_i = \theta_i - \Omega t$. This transforms Eq. 3 to

$$\dot{\phi}_i = (\omega_i - \Omega) + \lambda \sum_{j=1}^N a_{ij} \sin(\phi_j - \phi_i). \quad (\text{B1})$$

To simplify Eq. B1 further, we introduce the set of local order parameters defined by

$$r_i e^{i\psi_i} = \sum_{j=1}^N a_{ij} e^{i\phi_j}, \quad (\text{B2})$$

whose magnitude r_i can be interpreted as a measure of synchronization among the network neighbors of node i . We note that precisely k_i terms contribute to r_i , as thus $r_i \in [0, k_i]$, as opposed to the global order parameter r , which is bounded by one. Using the definition of the local order parameters, Eq. B1 simplifies to

$$\dot{\phi}_i = (\omega_i - \Omega) + \lambda r_i \sin(\psi_i - \phi_i). \quad (\text{B3})$$

Importantly, Eq. B3 can be used to classify the dynamics of each oscillator i given ω_i , r_i , ψ_i , Ω , and λ . If $|\omega_i - \Omega| \leq \lambda r_i$, then ϕ_i approaches a stable fixed point given by $\sin(\phi_i - \psi_i) = (\omega_i - \Omega) / \lambda r_i$. We refer to these oscillators as phase-locked, as the existence of a fixed fixed point corresponds to joining the synchronized population. On the other hand, if $|\omega_i - \Omega| > \lambda r_i$, then ϕ_i never reaches a fixed point and oscillator i drifts for all time, and thus we refer to these oscillators as drifting.

To classify the degree of synchronization, we next consider the family of local order parameters. We begin by neglecting the contribution of drifting oscillators to each r_i . This has been shown to be an accurate approximation in such correlated oscillators networks [44]. Equation (B2) can then be rewritten as

$$r_i = \sum_{|\omega_j - \Omega| \leq \lambda r_j} a_{ij} e^{i(\phi_j - \psi_i)}. \quad (\text{B4})$$

We now make two important simplifying assumptions. First, we assume that the average phases ψ_i and ψ_j of each pair of network neighbors (i, j) is approximately equal, i.e., $\psi_i \approx \psi_j$. This is a reasonable assumption when the synchronized solution consists of a single synchronized cluster, as is typically the case when the network structure is not strongly modular. Second, we recall the definition of the local order parameters in Eq. B2, noting that exactly k_i terms contribute to r_i . We propose that each r_i is proportional to its degree k_i , i.e., there exists some \tilde{r} such that $r_i \approx \tilde{r} k_i$ for all i . Both approximations are particularly accurate when the average nodal degree is not too small, thus improving the sampling of local averages. We note that these approximations have been used and verified in other synchronization literature [43–46]. Furthermore, it can be shown that the constant \tilde{r} is a good approximation for the global degree of synchronization r , and thus we will approximate $\tilde{r} \approx r$.

Next we expand the exponential in Eq. B4 into cosine and sine and use that at steady-state phase-locked oscillators satisfy $\sin(\phi_i - \psi_i) = (\omega_i - \Omega)/\lambda r_i$ to obtain

$$rk_i = \sum_{|\omega_j - \Omega| \leq \lambda r k_j} a_{ij} \left[\sqrt{1 - \left(\frac{\omega_j - \Omega}{\lambda r k_j} \right)^2} + i \frac{\omega_j - \Omega}{\lambda r k_j} \right]. \quad (\text{B5})$$

Finally, we sum Eq. B5 over all i , divide by N , and separate into real and imaginary parts to obtain, after some rearranging, the self consistency condition given in Eqs. 7 and 8. This system of equations jointly describe the steady-state synchronization dynamics given a sequence of degree-frequency pairs $\{(k_i, \omega_i)\}_{i=1}^N$ and can be solved self-consistently for r and Ω . In principle, the sums in Eqs. (7) and (8) can be transformed into integrals in the limit $N \rightarrow \infty$ given a joint distribution of degrees and frequencies $P(k, \omega)$. However, we find that the sum representation of Eqs. (7) and (8) suffices to describe the dynamics (see Fig. 4).

Appendix C: Additional figures

In the main text we showed that spontaneous synchronization emerges for a wide range of the biasing parameter α . Here we show that spontaneous synchronization emerges for many different combinations of network structures as well. We report here additional plots of the phase diagram, synchronization profiles, frequency distribution, and scaling of the stationary energy distribution p_k^* for all the combinations of two different topologies of the energy transport layer, namely an Erdős-Rényi graph with connection probability $p = 0.01$ (ER) and a scale-free configuration model random graph with $P(k) \sim k^{-\gamma}$ for $\gamma = 2.8$ (SF-2.8) and four different topologies of the synchronization layer graph, namely scale-free configuration model random graphs with $P(k) \sim k^{-\gamma}$ for $\gamma = 2.2, 2.5, 2.8, 3.0$ (respectively denoted SF-2.2, SF-2.5, SF-2.8 and SF-3.0).

In Fig. 5 we show the phase diagrams in the $\alpha - \lambda$ plane, for ER (left) and SF-2.8 (right) energy transport

layer and for increasing values of the exponent γ of the degree distribution of the synchronization layer. We note qualitatively equivalent behavior for all cases indicating that spontaneous synchronization is robust to all combinations of structure of the two layers. We always observe a sharp synchronization transition in an interval of positive values of α , usually between $\alpha \simeq 0.6$ and $\alpha \simeq 1.5$, even if the precise width of such interval depends on the topology of the two layers.

In Fig. 6 we compare some relevant cross-sections of these phase diagrams that correspond to the forward synchronization profiles for the ER transport layer for fixed (a) α and (b) λ . It is interesting to notice that, in addition to it being possible to control the degree of synchronization for fixed α by changing λ , for relatively wide ranges of fixed λ it is possible to control the degree of synchronization by changing α . Furthermore, for both cases for the transition between incoherence and synchronization is often sharp.

In Fig. 7 we show the distribution of natural frequency for the eight combinations of layer topologies reported in Fig. 5. In general, the qualitative behavior of the system is preserved, so that higher values of the motion bias correspond to broader distributions of frequencies. The quantitative difference between the case of ER and SF-2.8 energy transport layer (different exponents of $P(\omega)$) is due to the difference in the expected average degree of the first neighbors of a node in an Erdős-Rényi graph and in an uncorrelated scale-free network, which concurs to determine the shape of the distribution of frequencies. In fact, in the former case the average degree of the first neighbors of a node scales as $\langle k \rangle$ (which is a constant), while in the latter one it scales as $\langle k^2 \rangle / \langle k \rangle$ and depends on the exponent of the degree distribution of the energy transport layer.

Finally, in Fig. 8 we present the scaling of p^* with k for different values of the motion bias α for ER (left) and SF-2.8 (right) transport layers. We notice again that the qualitative behavior of p_k^* does not heavily depend on the topology of the energy transport layer, while the exponent of the degree distribution of the synchronization layer actually affects the magnitude of the fluctuations around the expected scaling.

-
- [1] Boccaletti S, Latora V, Moreno Y, Chavez M, Hwang D-U (2006) Complex networks: structure and dynamics. *Phys Rep* 424:175–308.
 - [2] Newman MEJ (2003) The structure and function of complex networks. *SIAM Review* 45:167–256.
 - [3] Strogatz SH (2001) Exploring complex networks. *Nature* 410:268–276.
 - [4] Newman M (2010) Networks: An Introduction. Oxford University Press, Oxford, UK.
 - [5] Barrát A, Barthélemy M, Vespignani A, (2008) Dynamical Processes on Complex Networks. Cambridge University Press, Cambridge, UK.
 - [6] Arenas A, Díaz-Guilera A, Kurths J, Moreno Y, Zhou C, (2008) Synchronization in complex networks. *Phys. Rep.* 469:93–153.
 - [7] Castellano C, Fortunato S, Loreto V, (2009) Statistical physics of social dynamics. *Rev. Mod. Phys.* 81:591–646.
 - [8] Roca CP, Cuesta JA and Sánchez A, (2009) Evolutionary game theory: Temporal and spatial effects beyond replicator dynamics. *Physics of Life Reviews* 6:208–249.
 - [9] Bullmore E, Sporns O (2009) Complex brain networks: graph theoretical analysis of structural and functional systems. *Nat Rev Neurosci* 10:186–198.
 - [10] Deco G, Jirsa VK, McIntosh AR (2013) Resting brains

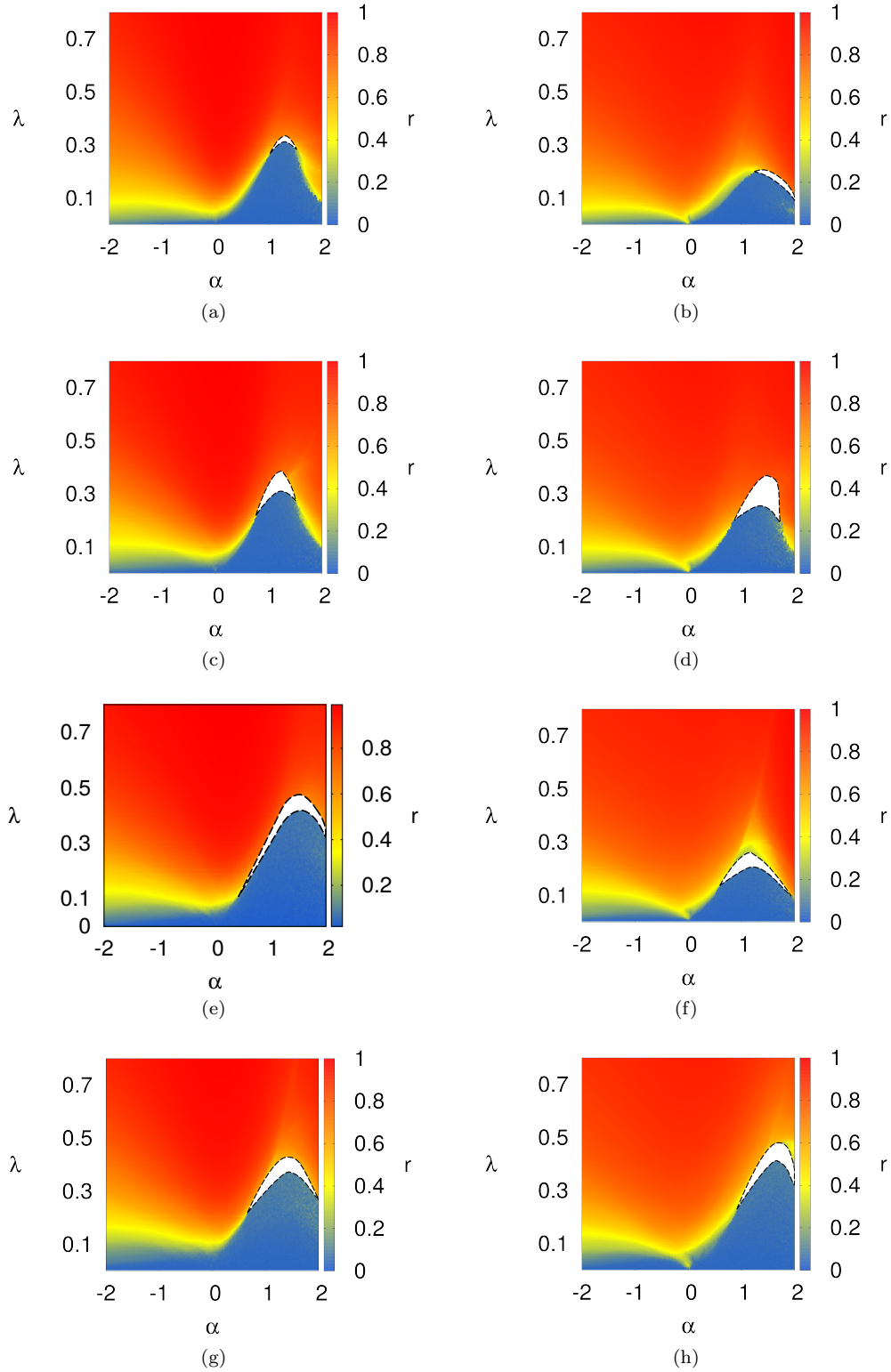


FIG. 5: Phase diagram of the system for different topologies of the energy transport layer (respectively, Erdős-Rényi on the left, scale-free configuration model random graphs with $P(k) \sim k^{-2.8}$ on the right) and of the synchronization layer (scale-free graphs with $P(k) \sim k^{-\gamma}$, with γ respectively equal to 2.2, 2.5, 2.8 and 3.0, from top to bottom). Independently of the actual combination of layer topologies, we always observe a relatively large interval of α in which the synchronization transition is abrupt.

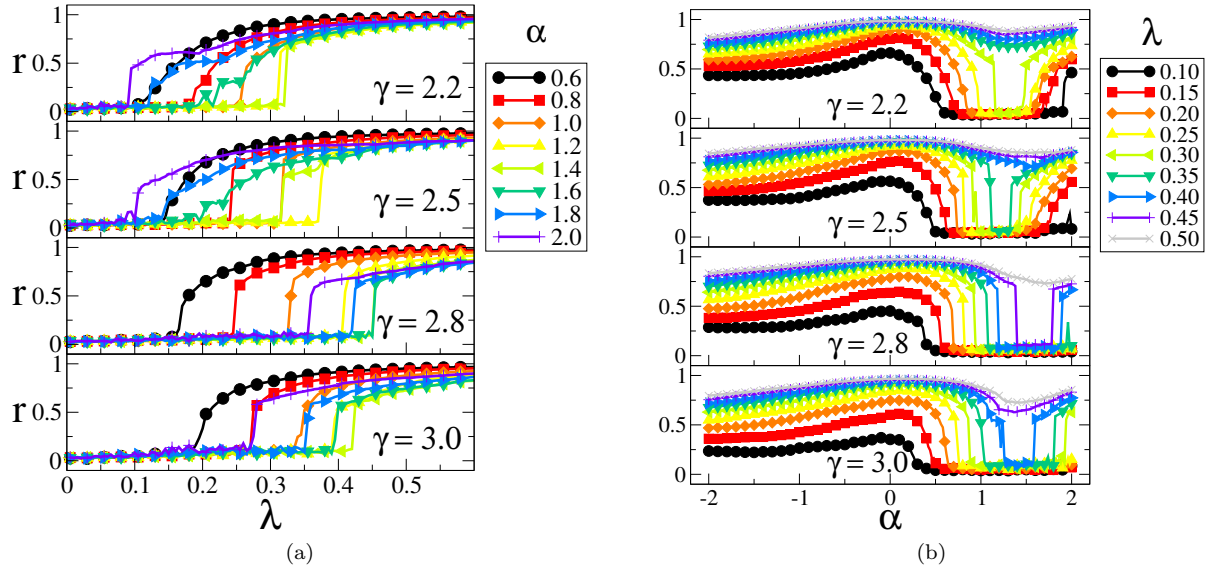


FIG. 6: (a) Forward synchronization diagrams corresponding to different values of the motion bias α and different exponents of the scale-free degree distribution on the synchronization layer (the energy transport layer is an Erdős-Rényi graph with $p = 0.01$). It is evident that the actual interval of α values in which we observe a sharp synchronization transition actually depends on the topology of the synchronization layer. (b) Cross-section of the phase diagrams reported in Fig. 5 (left) for different fixed values of λ as a function of α . Interestingly, it is possible to force the system either in a incoherent or synchronized state not only by tuning the coupling strength λ , but also the motion bias α . Notice that for some values of λ the transition to synchronization as a function of α is sharp.

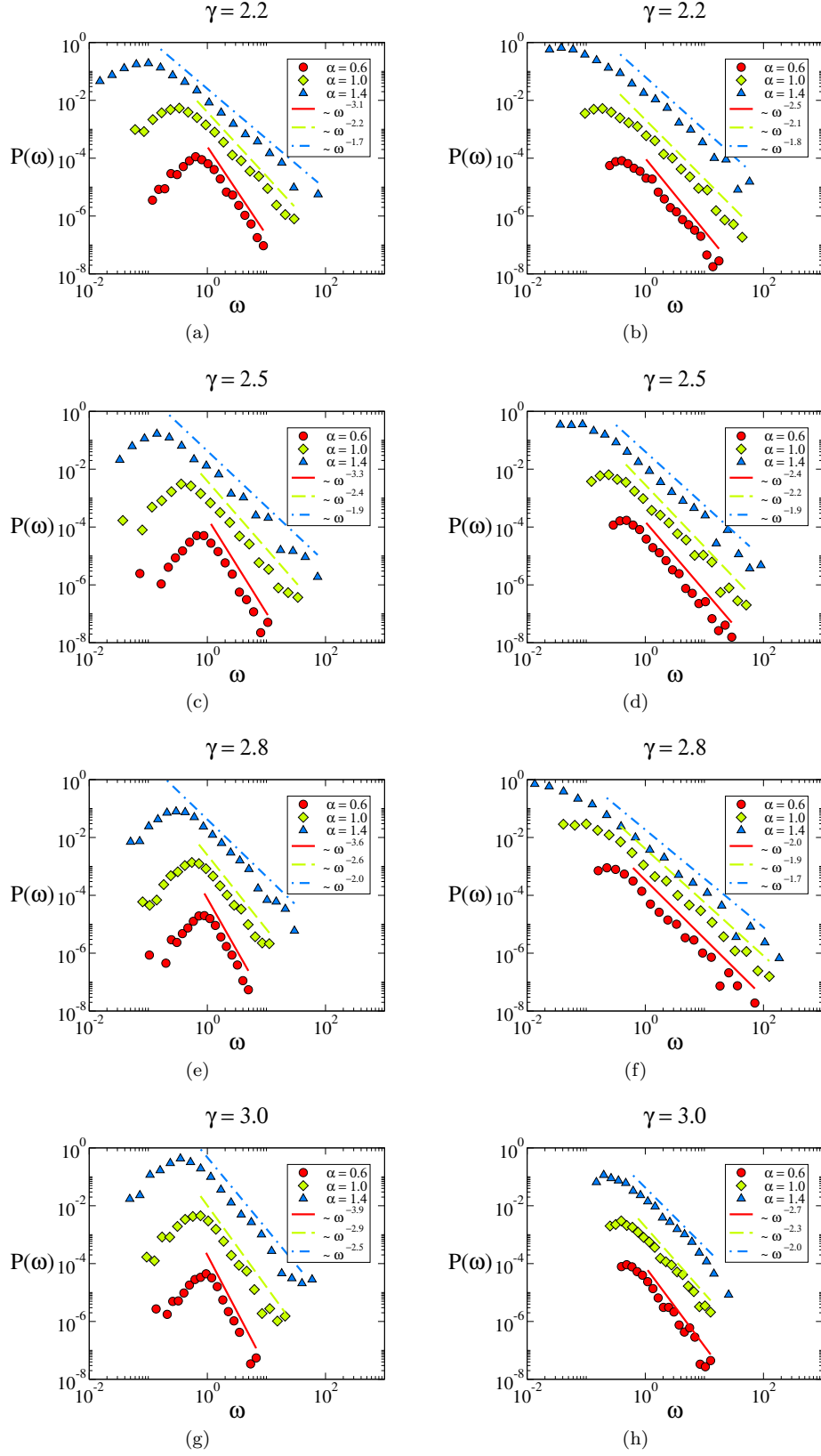


FIG. 7: The distribution of natural frequencies, as induced by the distribution of random walkers on an Erdős-Rényi (left) and a scale-free energy transport layer (right) for several values of α and different exponents of the degree distribution at the synchronization layer. The qualitative behavior of the distribution remains the same: it has a broad power-law-like tail independently of the topology of the two layers, and the major effect of different topologies is just a tuning of the exponent of this tail. Remarkably, higher values of α contribute to the broadening of the distribution $P(\omega)$.

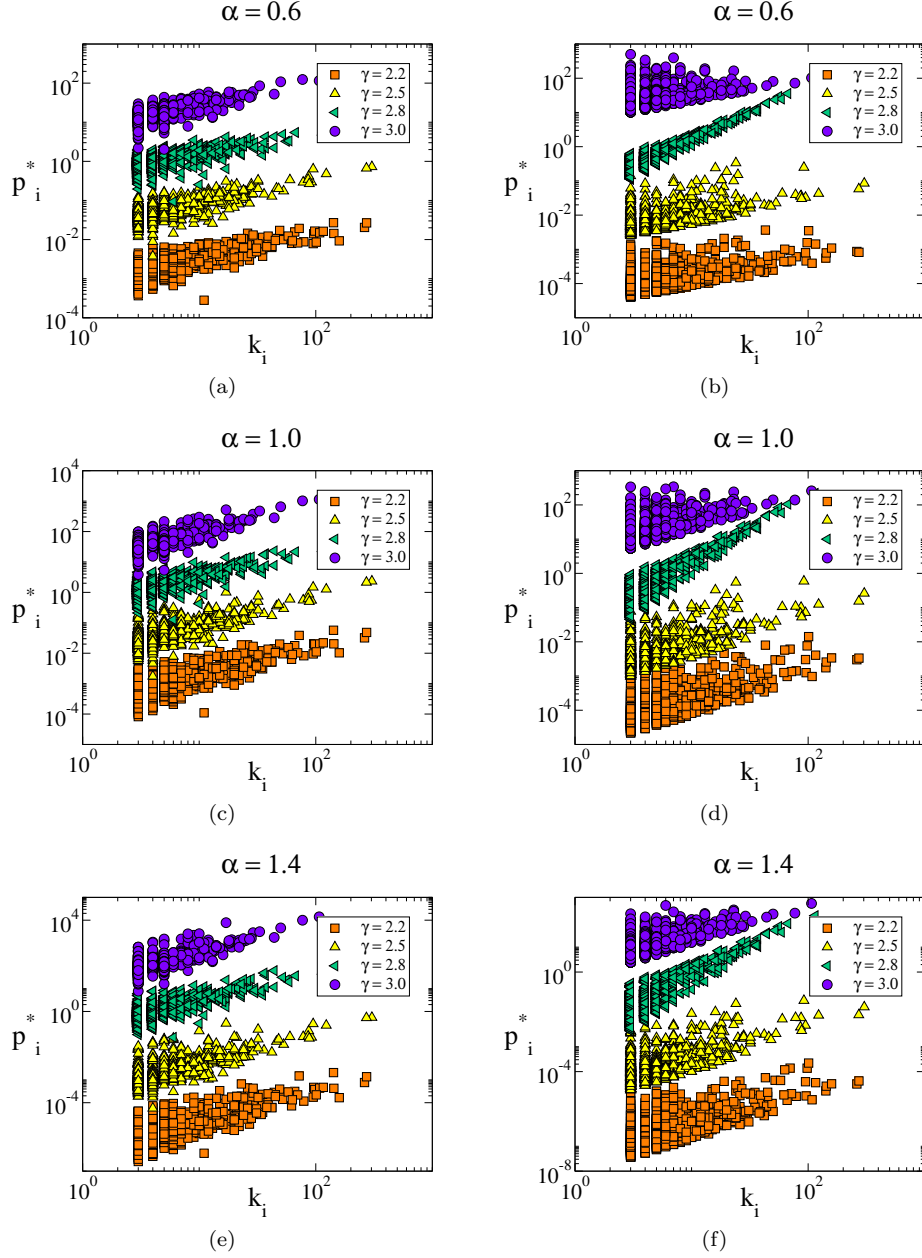


FIG. 8: Scaling of the stationary node occupation probability p^* for Erdős-Rényi (left) and scale-free (right) energy transport layers, different values of α and different values of the exponent γ of the degree distribution on the synchronization layer. The major visible effect of the heterogeneity of the synchronization layer on the scaling of p^* as a function of k is an attenuation of the fluctuations when γ increases.

- never rest: computational insights into potential cognitive architectures. *Trends Neurosci* 36:268–274.
- [11] Nicosia V, Valencia M, Chavez M, Diaz-Guilera A, Latora V (2013) Remote synchronization reveals network symmetries and functional modules. *Phys. Rev. Lett.* 110:174102.
 - [12] Buldyrev SV, Parshani R, Paul G, Stanley HE, Havlin S (2010) Catastrophic cascade of failures in interdependent networks. *Nature* 464:1025–1028.
 - [13] Granell C, Gomez S, Arenas A (2013) Dynamical interplay between awareness and epidemic spreading in multiplex networks. *Phys Rev Lett* 111:128701.
 - [14] Kivelä M, Arenas A, Barthélemy M, Gleeson JP, Moreno Y and Porter MA, (2013) Multilayer networks. arXiv:1309.7233.
 - [15] Boccaletti S, Bianconi G, Criado R, del Genio CI, Gómez-Gardeñes J, Romance M, Sendiña-Nadal I, Wang Z and Zanin M (2014) The structure and dynamics of multilayer networks. arXiv:1407.0742.
 - [16] Goldbeter A, Koshland DE (1981) An amplified sensitivity arising from covalent modification in biological systems. *Proc Natl Acad Sci USA* 78(11):6840.
 - [17] Brandman O, Ferrell JE, Li R, Meyer T (2005) Interlinked fast and slow positive feedback loops drive reliable cell decisions. *Science* 310:496.
 - [18] Kim SY, Ferrell JE (2007) Substrate competition as a source of ultrasensitivity in the inactivation of Wee1. *Cell* 128(6):1133.
 - [19] Siegal-Gaskins D, Mejia-Guerra MK, Smith GD, Grote-wold E (2011) Emergence of switch-like behavior in a large family of simple biochemical networks. *PLoS Comput Biol* 7(5):e1002039.
 - [20] Verbrugge LM (1979) Multiplexity in adult friendships. *Social Forces* 57:1286–1309.
 - [21] Wasserman S, Faust K (1994) *Social Network Analysis: Methods and Applications* (Cambridge University Press).
 - [22] Gómez S, Díaz-Guilera A, Gómez-Gardeñes J, Pérez-Vicente CJ, Moreno Y, and Arenas A (2013) Diffusion dynamics on multiplex networks. *Phys. Rev. Lett.* 110:028701.
 - [23] Nicosia V, Bianconi G, Latora V, Barthélemy M (2013) Growing multiplex networks. *Phys Rev Lett* 111:058701.
 - [24] De Domenico M, et al. (2013) Mathematical formulation of multilayer networks. *Phys Rev X* 3:041022.
 - [25] Battison F, Nicosia V, Latora V (2014) Structural measures for multiplex networks, *Phys Rev E* 89:032804.
 - [26] Gómez-Gardeñes J, Latora V (2008) Entropy rate of diffusion processes on complex networks. *Phys Rev E* 78:065102.
 - [27] Kuramoto Y (1984) *Chemical Oscillations, Waves, and Turbulence* (Springer, New York).
 - [28] Edvinsson L, Krause DN Eds (2002) *Cerebral Blood Flow and Metabolism, 2nd Edition* (Williams & Wilkins, Philadelphia).
 - [29] Malonek D, et al. (1997) Vascular imprints of neuronal activity: Relationships between the dynamics of cortical blood flow, oxygenation, and volume changes following sensory stimulation. *Proc Natl Acad Sci USA* 94(26):14826–14831.
 - [30] Sheth SA, et al. (2004) Linear and nonlinear relationships between neuronal activity, Oxygen metabolism, and hemodynamic responses. *Neuron* 42(2):347–355.
 - [31] Allen EA, Pasley BN, Duong T, Freeman RD (2007) Transcranial magnetic stimulation elicits coupled neural and hemodynamic consequences. *Science* 317(5846):1918–1921.
 - [32] Erdős P, Rényi A (1960) On the evolution of random graphs. *Pub Math Inst Hung Acad Sci* 5:17–61.
 - [33] Bekessy A, Bekessy P, Komlos J (1972) Asymptotic enumeration of regular matrices. *Stud Sci Math Hung* 7:343–353.
 - [34] Gómez-Gardeñes J, Gómez S, Arenas A, Moreno Y (2011) Explosive synchronization transitions in scale-free networks. *Phys Rev Lett* 106:128701.
 - [35] Leyva I, et al. (2013) Explosive transitions to synchronization in networks of phase oscillators. *Sci Rep* 3:1281.
 - [36] Zhang X, Hu X, Kurths J, Liu Z (2013) Explosive synchronization in a general complex network. *Phys Rev E* 88:010802(R).
 - [37] Iadecola C (1998) Neurogenic control of the cerebral microcirculation: is dopamine minding the store? *Nat. Neurosci.* 1:263–265.
 - [38] Krimer LS, Muly EC, Williams GV, Goldman-Rakic PS (1998) Dopaminergic regulation of cerebral cortical microcirculation. *Nat Neurosci* 1:286–289.
 - [39] Raichle ME, et al. (2001) A default mode of brain function. *Proc Natl Acad Sci USA* 98:676–682.
 - [40] Greicius MD, Krasnow B, Reiss AL, Menon V (2002) Functional connectivity in the resting brain: A network analysis of the default mode hypothesis. *Proc Natl Acad Sci USA* 100(1):253–258.
 - [41] Goñi J, et al. (2013) Resting-brain functional connectivity predicted by analytic measures of network communication. *Proc Natl Acad Sci USA* 111(2):833.
 - [42] Honey CJ, Kötter R, Breakspear M, Sporns O (2007) Network structure of cerebral cortex shapes functional connectivity on multiple time scales. *Proc Natl Acad Sci USA* 104(24):10240–10245.
 - [43] Skardal PS, Sun J, Taylor D, Restrepo JG (2013) Effects of degree-frequency correlations on network synchronization: Universality and full phase-locking. *Europhys Lett* 101:20001.
 - [44] Skardal PS, Arenas, A (2014) Disorder induces explosive synchronization. *Phys Rev E* 89:062811.
 - [45] Ichinomiya T (2004) Frequency synchronization in random oscillator networks. *Phys Rev E* 70:026116.
 - [46] Restrepo JG, Ott E, Hunt BR (2005) Onset of synchronization in large networks of coupled oscillators. *Phys Rev E* 71:036151.